

¹ Self-Deployable, Adaptive Soft Robots Based on Contracting-Cord Particle Jamming

³ Wenzhong Yan^{1,2*}, Brian Ye¹, Mingxi Li²,
⁴ Jonathan B. Hopkins¹, and Ankur Mehta²

⁵ ¹ Mechanical and Aerospace Engineering Department, UCLA, USA

⁶ * wzyan24@g.ucla.edu

⁷ ² Electrical and Computer Engineering Department, UCLA, USA

⁸ **Abstract.** We developed a new class of soft locomotive robots that can
⁹ self-assemble into a preprogrammed configuration and vary their stiffness
¹⁰ afterward in a highly integrated, compact body using contracting-cord
¹¹ particle jamming (CCPJ). We demonstrate this with a tripod-shaped
¹² robot, TripodBot, comprising of three CCPJ-based legs attached to a
¹³ central body. TripodBot is intrinsically soft and can be stored and trans-
¹⁴ ported in a compact configuration. On site, it can self-deploy and crawl in
¹⁵ a slip-stick manner through the shape morphing of its legs; a simplified
¹⁶ analytical model accurately captures the speed. The robot's adaptability
¹⁷ is demonstrated by its ability to navigate tunnels as narrow as 61% of
¹⁸ its deployed body width and ceilings as low as 31% of its freestanding
¹⁹ height. Additionally, it can climb slopes up to 15 degrees, carry a load
²⁰ of 5 grams (2.4 times its weight), and bear a load 9429 times its weight.

²¹ **Keywords:** contracting-cord particle jamming, self-deployment, adap-
²² tive robots, soft robots, tunable stiffness

²³ 1 Introduction

²⁴ Locomotive robots capable of self-assembly and post-deployment stiffness and
²⁵ shape variance are of great interest[1]. These robots hold vast potential for ap-
²⁶ plications in exploration within complex and remote areas, where they can be
²⁷ transported in compact conformations and deployed into preprogrammed con-
²⁸ figurations for meaningful onsite tasks[2]. Due to their tunable shape and stiff-
²⁹ ness[3], such robots can adapt to complex environments, such as exploring nar-
³⁰ row gaps in rubble [4]. However, creating such self-deployable, adaptive robots
³¹ remains a significant challenge, notwithstanding its importance.

³² Recently, there has been increasing interest towards achieving this goal[5–
³³ 8]. Drawing inspiration from biological organisms, soft robots are designed to
³⁴ achieve high flexibility and environmental adaptability due to their composition
³⁵ of primarily compliant materials[9]. To enhance the load-carrying capacity and
³⁶ structural rigidity of soft robots, various variable-stiffness mechanisms have been

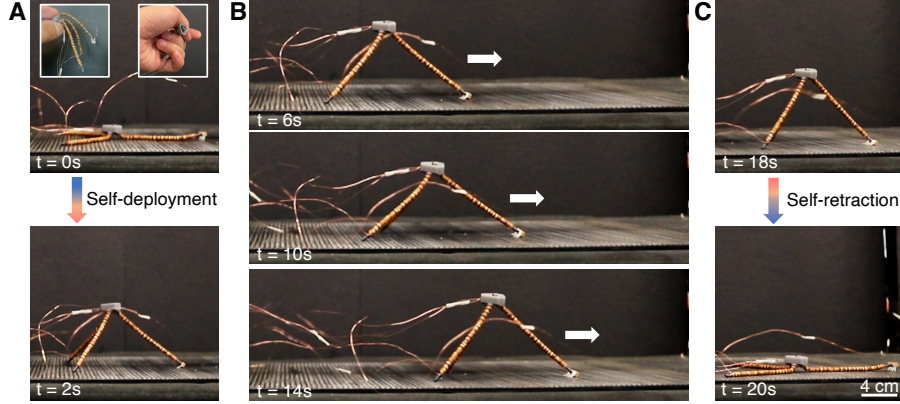


Fig. 1. The TripodBot in action. (A) The TripodBot can self-assemble from a soft, compact state to a preprogrammed tripod shape with certain rigidity. (B) After deployment, it can crawl in a slip-slick manner. (C) After finishing the task, it can collapse back to soft state, ready for the next deployment.

37 proposed, including low-melting-point alloys [10], magnetorheological fluids [11],
 38 and antagonistic actuation [12]. These methods often require the integration
 39 of multiple actuators with coordinated control [12] or the addition of passive
 40 variable-stiffness modules alongside actuation modules for shape change [13].
 41 Such integrations lead to bulky robotic systems [14] and complex control archi-
 42 tectures [15]. Although these approaches offer greater system flexibility, allowing
 43 independent control of robots' stiffness and shape, they are challenging to in-
 44 incorporate into locomotive robots, especially at the centimeter scale. Therefore,
 45 there is a strong need to develop self-deployable, adaptive soft robots utilizing a
 46 single actuation system to minimize implementation complexity and weight.

47 Here, we introduce a new class of soft robots that can self-deploy and ad-
 48 just both shape and stiffness post-assembly in a highly integrated manner.
 49 These robots build upon our previous work on contracting-cord particle jam-
 50 ming (CCPJ) [3]. The CCPJ mechanism primarily involves contracting actu-
 51 ators threaded through beads with matching interfaces in networked chains with
 52 initial slack. When the contracting actuators are activated, the beads gather
 53 into preprogrammed configurations, and further contraction tunes the stiffness
 54 of the assemblies, similar to common material jamming [16, 17]. Compared to
 55 vacuum-driven active particle jamming [1], CCPJ offers several advantages: (1) it
 56 is easier to fabricate without requiring airtight sealing, and thus provides higher
 57 scalability; (2) it does not require bulky associated components, such as pumps
 58 and valves, for untethered operation; and (3) it is robust to punctures, which
 59 are difficult to avoid in complex, restricted areas.

60 We demonstrate the capabilities of this technology with a tripod-shaped
 61 robot, TripodBot, featuring three CCPJ-based legs attached to a central body
 62 (Fig.1). We harness shape memory alloys (SMA) as main contracting-cord ac-

tuators. TripodBot is intrinsically soft and can be stored and transported in a compact configuration. Once deployed, it crawls using slip-stick locomotion facilitated by the shape morphing of its legs. The locomotion speed of TripodBot varies with changes in the actuation period, reaching a maximum speed of approximately 0.51 m/min (7.5 BL/min), accurately predicted by a simplified analytical model. The robot's adaptability is showcased by its ability to navigate tunnels as narrow as 61% of its deployed body width and ceilings as low as 31% of its freestanding height. This adaptability is prominent among similar robots[4]. Additionally, TripodBot can climb slopes up to 15 degrees and carry a load of 5 grams (2.4 times its own weight). It can also bear a load, 9429 times its weight when incorporating super-coiled polymer (SCP) actuators[18] instead of SMA wires. This work offers a practical framework for designing soft robots with self-deployability, adaptability, and load-carrying capability, suitable for exploration in remote and complex areas.

Specifically, the contributions of this paper include:

1. a locomotion mechanism through the combination of directional friction and shape-changing of CCPJ mechanism,
2. a method that enables adaptive locomotion and load-carrying through CCPJ, and
3. a soft crawling robot fabricated out of the proposed design and verified by experiments.

The remainder of the paper is organized as follows: in Section 2, we briefly introduce the CCPJ mechanism; in Section 3, we introduce the design, fabrication, and control of TripodBot; in Section 4, we demonstrate the performance of TripodBot; and the conclusion is presented in Section 5.

2 CCPJ for Self-Deployment and Stiffness Variance

CCPJ structures are the main components for constructing our self-deployable, adaptive robots. Therefore, we will introduce the fundamental mechanism and basic characteristics of CCPJ structures here, preparing the design of our robots. CCPJ structures are comprised of contracting actuators threaded through beads with matching interfaces in networked chains[3]. The fundamental unit is a straight CCPJ beam as the leg of the TripodBot (Fig.1). Therefore, we use this straight beam as an example to show the characteristics of CCPJ structures. As shown in Fig.2, the slack network conforms to arbitrary shapes, but when actuated, it self-assembles into a preprogrammed configuration with beads gathered together. Further contraction of the actuators can dynamically tune the assembly's mechanical properties through the beads' particle jamming, while maintaining the overall structure with minimal change.

2.1 Design, Fabrication, and Experimental validation of CCPJ

The CCPJ beam (Fig.2A) mainly consists of 20 beads (3 mm thickness, plywood) threaded through the central hole by a SMA wire of 0.15 mm diameter

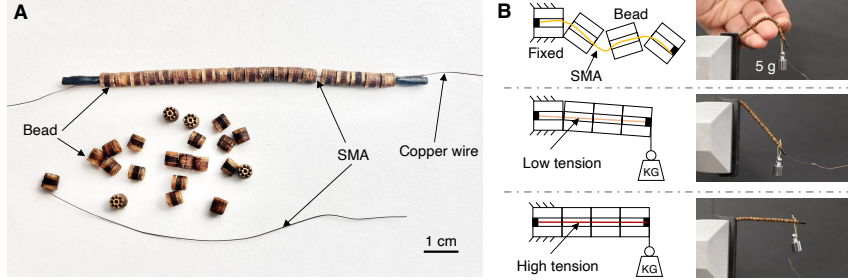


Fig. 2. Design and fabrication of a CCPJ beam. (A) The beam is composed of 20 beads threaded through with a SMA wire. Each assembled beam weights 0.46 g. (B) After applying current across the SMA wire, the beam can self-deploy and continuously increases its stiffness as the current increase. One beam with a current of 0.4 A can hold a 5 g weight.

(Biometal). Two ends of the SMA wire are connected to an electrical power source through copper wires and fixed firmly to specify the length with heat shrinking tubes. Here we chose to use SMA given the potential for untethered operation with widely available electrical control and power[19]. Other contracting actuator can be used for different goals. Each beam has an initial slack of 1.6 mm, which means the length of the SMA wire is 1.6 mm longer than the total length of the 20 beads. Therefore, the CCPJ beam is soft before actuation (Fig.2B). When current is applied to the SMA wire, the beads conform to the preprogrammed straight configuration with certain compliance. As the current increases, the beam becomes stiffer and can sustain a 5 gram weight with minimal deflection (about 11 times its own weight, Fig.2B).

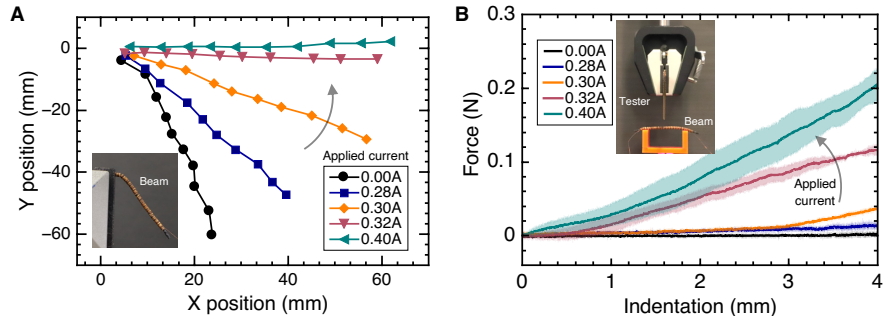


Fig. 3. Characterization of a CCPJ beam. (A) The curvatures of the horizontally clamped beam against gravity with varying applied current on the SMA wire. (B) The force-indentation relationship changes over the applied current. Shaded areas represent SD over three tests.

115 **2.2 Self-Deployment of CCPJ Beam**

116 To quantitatively evaluate the self-deployment of the CCPJ beam, we clamped
 117 the beam horizontally against gravity(Fig.3A). We recorded the shapes of the
 118 CCPJ beam under various current ranging from 0 A to 0.4 A. Then we extracted
 119 the curvatures of the beam using *Tracker* and plotted them in Fig.3A. When
 120 the current reached 0.32A, the beam became straight. Increasing current did
 121 not change the shape, however, the rigidity of the beam can be increased(see the
 122 next section). Here, we only consider the effect of gravity on the beam. Different
 123 loading conditions can change how the shape evolution along the change of the
 124 applied current.

125 **2.3 Stiffness Variation of CCPJ Beam**

126 To characterize the stiffness of the CCPJ beam under different currents, we
 127 employed a mechanical tester (Mecmesin). The indenter of the tester moved
 128 downward at a speed of 6 mm/min and measured the force acted upon the
 129 indenter in the vertical direction. The tested CCPJ beam was simply supported
 130 by two acrylic beams with a distance of 40 mm (Fig.3B). We measured the
 131 force-indentation curves of the CCPJ beam under nine different current levels.
 132 For each current level, we repeated the test three times to obtain the average
 133 force-indentation curves. The shaded areas in Fig.3B represents the SD. Between
 134 each test, we manually straightened the beam.

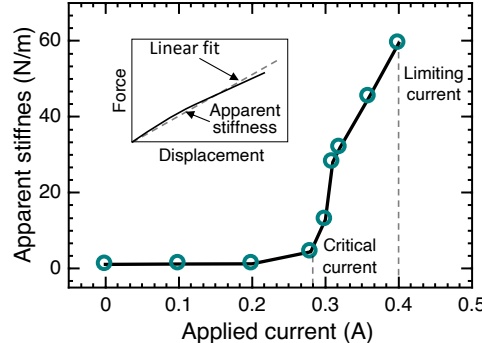


Fig. 4. Apparent stiffness variance over applied current of a CCPJ beam.
 The stiffness can increase by 53.7 times when the current changes from 0 A to 0.4 A.

135 The results show that the stiffness of the beam increased monotonically with
 136 the increasing current. The elasticity of the whole beam was rather linear within
 137 our deflection range (0–4 mm). The apparent bending stiffness of the CCPJ beam
 138 under various applied currents was calculated and is summarized in Fig.4. As the
 139 current increased from 0 to 0.4 A, the apparent bending stiffness of the structure

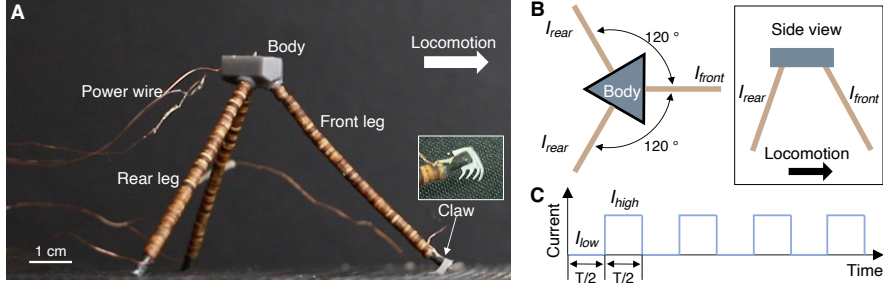


Fig. 5. Design and control of the TripodBot. (A) Picture of the TripodBot with labels. (B) The top view and side view of the robot. (C) Typical control signal: square wave with a duty cycle of 1/2.

exhibited a rapid increase from 1.1 to 59.1 N/m with a 53.7 times increase. Note that, when the current exceeded 0.28 A, this apparent bending increase became much more pronounced. This binary behavior is typical for SMA actuators[20, 21]. We also noticed that the stiffness increase did not reach a plateau when the current became 0.4 A. However, we did not increase the current beyond 0.4 A since higher current can make SMA unstable and fatigue quickly over time[19].

146 3 Design and Fabrication of the TripodBot

147 We designed a tripod-shaped robot with three CCPJ straight beams to exemplify
148 our CCPJ-based robots. This configuration is simple to fabricate and control.
149 It also provides potential for omnidirectional locomotion for future development
150 for field applications.

151 3.1 Design and Control for Locomotion

152 The TripodBot consists of three legs that are connected to a central body
153 (Fig.5A). The front leg has a specially designed claw that has anisotropic friction
154 between the forward and backward movements. When sliding forward, the claw
155 generates negligible friction, while preferably providing infinite friction when
156 moving backward. The two rear legs have relatively pointy tips that also can
157 provide anisotropic friction when interacting with the ground. The three legs
158 are evenly distributed around the body, with the front leg pointing to the direc-
159 tion of locomotion (Fig.5B). To make the control for locomotion simple, we used
160 a square wave with a duty cycle of 1/2 (Fig.5C). We grouped three legs into two
161 subgroups. Two rear legs are grouped together, while the front leg is controlled
162 individually. This design is to enable different locomotion gaits while remaining
163 relatively simple.

¹⁶⁴ **3.2 Fabrication and Assembly**

¹⁶⁵ Three identical straight legs of 65 mm long are attached to the body, with the
¹⁶⁶ tiled angles against the ground as 60°. The current is applied across the SMA
¹⁶⁷ wires through thin copper wires, which reduces their drag on the locomotion of
¹⁶⁸ the robot. An origami claw was laser cut and attached on the low end of the front
¹⁶⁹ leg to increase the asymmetry of friction for better locomotion[22]. Similarly,
¹⁷⁰ the tips of the rear legs were sharpened to improve the performance.

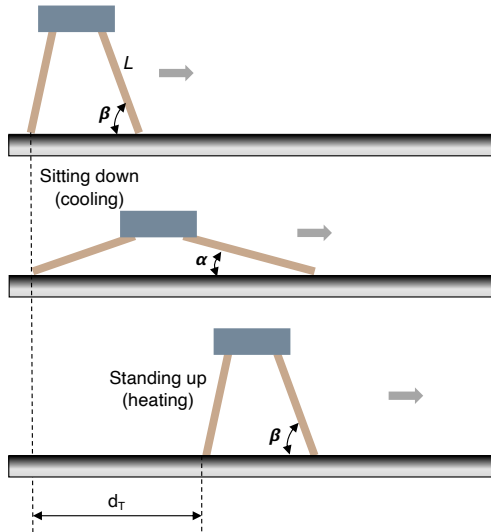


Fig. 6. Locomotion mechanism of the TripodBot.

¹⁷¹ **3.3 Simplified Analytical Model**

¹⁷² To better understand the mobility of the robot, we built a simplified analytical
¹⁷³ model of its motion (Fig.6). The robot has three legs with length L . We assume
¹⁷⁴ the robot performs perfect stick-slip crawling on the ratchet substrate with two
¹⁷⁵ strokes. In the first stroke, all the three legs are softened simultaneously. Both
¹⁷⁶ of the rear legs hold onto anchor positions without slipping backward, while
¹⁷⁷ the body and front legs move forward. In the second stroke, all three legs are
¹⁷⁸ tightened, and the robot stands up again. We assume that the front leg can
¹⁷⁹ firmly grasp the ground without slipping backward, and thus the body and rear
¹⁸⁰ legs are pulled forward. The contact angle of the front leg with the ground is
¹⁸¹ β when standing up and is α when sitting down. In addition, we assume that
¹⁸² all legs remain straight all the time. During the sitting down process, the robot
¹⁸³ moves for a distance of

$$d_d = \frac{L(\cos\alpha - \cos\beta)}{2} \quad (1)$$

¹⁸⁴ while it can move forward with a distance of d_u when stands up again

$$d_u = L(\cos\alpha - \cos\beta) \quad (2)$$

¹⁸⁵ Therefore, the speed of the robot is

$$v = \frac{d_T}{T} = \frac{d_d + d_u}{T} = \frac{3L(\cos\alpha - \cos\beta)}{2T} \quad (3)$$

¹⁸⁶ The contact angles, α and β , are dominantly determined by a complex inter-
¹⁸⁷ action between the legs, gravity, and ground. Because of the design, the maxi-
¹⁸⁸ mum contact angle of β for TripodBot is 60° and α can vary from 0 to 60° .

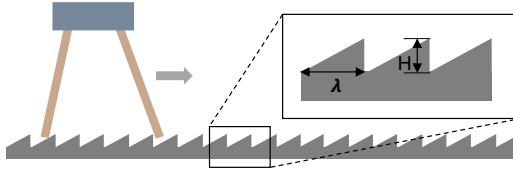


Fig. 7. Locomotion of the TripodBot on a ratchet surface.

¹⁸⁹ 4 Robot Demonstrations

¹⁹⁰ In this section, we demonstrate the functionality—locomotion, slope climbing,
¹⁹¹ adaptability, and load carrying—of the TripodBot. For simplicity and better
¹⁹² locomotion speed, we choose to have the I_{high} and I_{low} of the control current
¹⁹³ as 0.4 A and 0 A according to the result from the characterization of a CCPJ
¹⁹⁴ beam.

¹⁹⁵ 4.1 Self-Deployment and Self-Retraction

¹⁹⁶ As shown in Fig.1A, the robot is initially soft and can be stored compactly.
¹⁹⁷ After supplying the current, the robot can self-deploy into the designed tripod
¹⁹⁸ shape. The geometric bounding box of the robot changes from $15 \times 17 \times 73$ mm³
¹⁹⁹ (minimal) to $105 \times 120 \times 64$ mm³ (about 43 times larger). After the task, e.g.,
²⁰⁰ locomotion, the robot can collapse back to the soft state for easy and efficient
²⁰¹ storage and transportation.

²⁰² 4.2 Directional Crawling

²⁰³ Through the stick-slip mechanism, the TripodBot can directionally crawl on the
²⁰⁴ ground. We fabricated a ratchet surface (λ : 3.0 mm, H : 0.5 mm, see Fig. 7)
²⁰⁵ to facilitate the locomotion. We took videos and analyzed them with the video

206 analyzer tool *Tracker* to plot the displacement and calculate average speed.
 207 When the actuation period, T , is 4.0 s, the robot can crawl across a distance of
 208 209 mm with an average speed of 8.5 mm/s or 7.5 BL/min (Fig.8). By varying
 210 the actuation period from 2 s to 10 s, we showed that the robot have different
 211 locomotion speeds, reaching a maximum value at about $T = 4$ s (Fig.9).

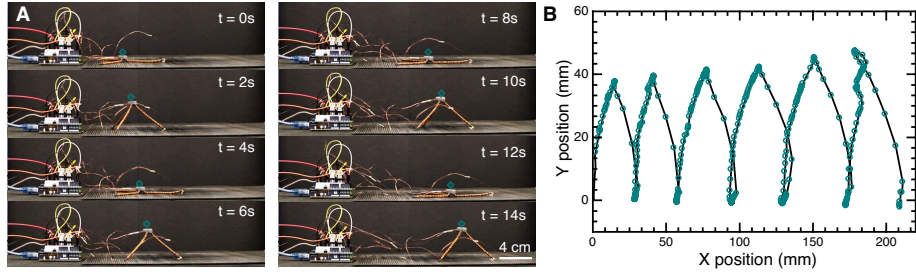


Fig. 8. Locomotion of the TripodBot with an actuation period of 4 s and applied current of 0.4A. (A) Snapshots. (B) Trajectory of the robot.

211 We compared analytical and experimental results, which were all in good
 212 agreement (Fig.9B). The values of β were measured directly from tests for the
 213 simplified analytical model. Since the robot sits down fully to the ground with
 214 the selected control signal. The contact angle α is 0. Then according to Eq.3,
 215 the speed of the robot is

$$v = \frac{3L(1 - \cos\beta)}{2T} \quad (4)$$

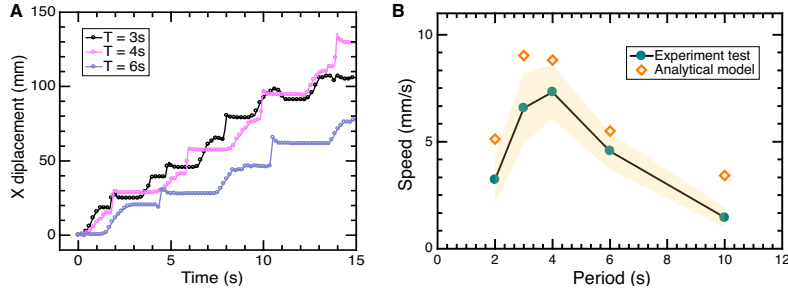


Fig. 9. Locomotion performance of the robot over actuation period. (A) X displacement as a function of time over different actuation periods. (B) Speed over actuation period.

216 We observed that the increase in β became significantly less pronounced and
 217 approached a plateau when the actuation period exceeded 4 s. Consequently,

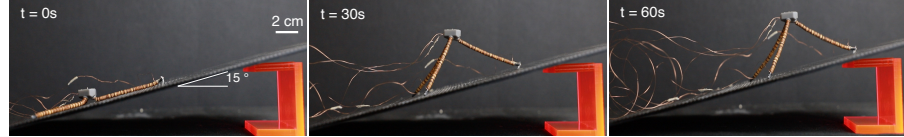


Fig. 10. Slope climbing. The average speed is 2.4 mm/s for a slope angle of 15°.

extending the actuation period results in a reduction of the average speed. Conversely, when the period decreased below 2s, the SMA wires did not have sufficient time to heat up and/or cool down, thereby failing to generate notable locomotion. Additionally, the values predicted by the analytical model should be considered as upper bounds, as real-world tests consistently exhibit some degree of slippage.

4.3 Slope Climbing

The TripodBot is capable of crawling on horizontal planes as well as locomoting on inclined surfaces, thereby expanding its range of applicable environments. We demonstrated this capability by showing it climbing a slope with a 15° incline. The robot can walk across a distance of 144 mm in 60 s with an average speed of about 2.4 mm/s. This ability shows the versatility of TripodBot for real-life deployment in various terrains.

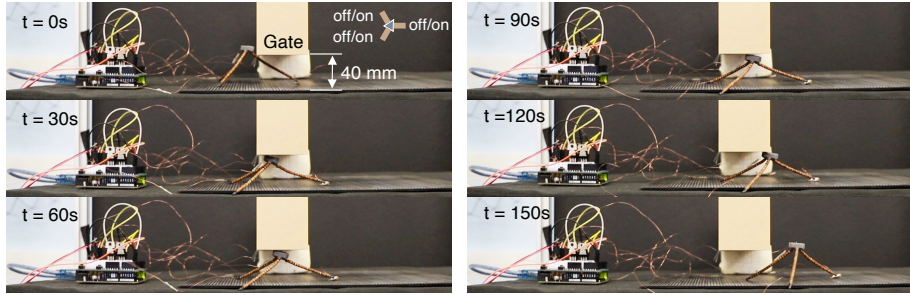


Fig. 11. The robot navigating through a confined space with the gap limit of 40 mm. The gap is 63% of the robot's height (63.5 mm).

4.4 Adaptive Navigation in Restricted Spaces

Owing to the inherent softness and shape-morphing ability of the TripodBot, it can adapt its shape to the restricted environment, albeit with a reduction in its speed. We showed this adaptability by illustrating the capability to navigate

235 through a series of restricted spaces. We first showed the robot can crawl at a
 236 relatively high speed in an open area and then lower its height to accommodate
 237 a 40 mm (63% height) gate by reducing the applied current to 0.38 A (Fig. 11).

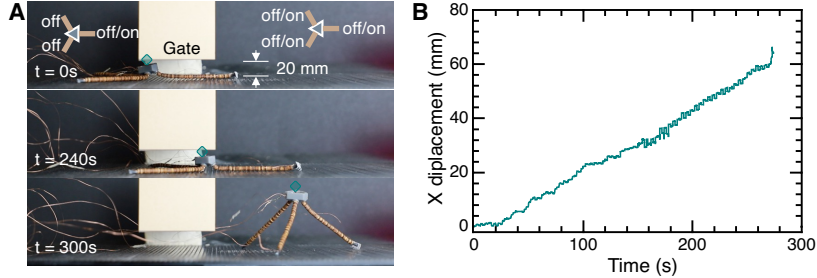


Fig. 12. The robot navigating through a confined space with the gap limit of 20 mm. (A) The snapshots. (B) The displacement over time. The gap is 31% of the robot's height (63.5 mm). Only the front leg was actuated within the space.

238 Then, we showed that the robot can locomote through an even lower gate of
 239 20 mm height (31% height, Fig. 12). However, we needed to modify the control
 240 signal to only activate the front leg. Lastly, we showed that the TripodBot can
 241 navigate a narrow tunnel with a cross-section area of 40×20 mm (61% width
 242 and 31% height of the fully deployed TripodBot) again only activating the front
 243 leg. This capability is among the best performance of similar robots [4].

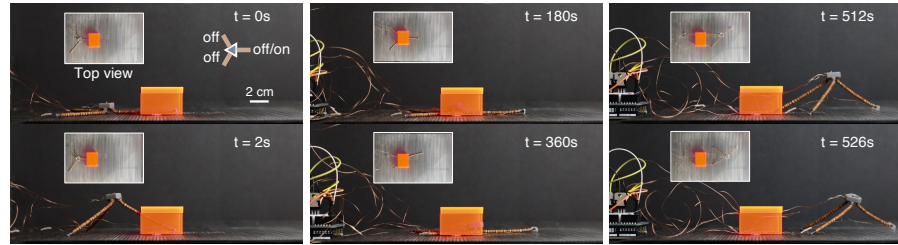


Fig. 13. The robot navigating through a confined tunnel with gap limit of 40×20 mm. The robot's height and width are 63.5 mm and 66 mm, respectively. Only the front leg was actuated within the tunnel.

244 4.5 Load Carrying

245 Loading capability is of significance for locomotive robots. The TripodBot is ca-
 246 pable of locomotion while carrying a 5 g (2.4 times its weight) mass, as shown

in Fig. 14. This capability indicates the potential to integrate on-board power, control, and sensors to allow untethered operation in restricted areas. In addition, the robot can statically sustain load up to 10 g (4.8 times of its weight) with all three legs supplied with 0.4 A current. This stiffening shows potential for energy absorption for various applications, e.g., temporary protection from falling objects [3, 23].

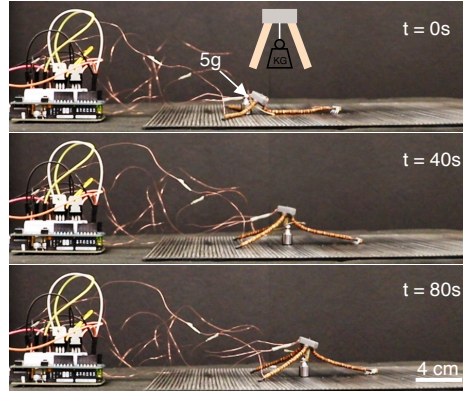


Fig. 14. Load carrying. The average speed is 0.34 mm/s with a load of 5 g (2.4 times its weight).

4.6 Robustness and Load Bearing

Robustness is essential for the survival of robots in complex environments [24]. The TripodBot presented here also has exceptional robustness characteristics, resulting from the assembly of soft materials with simple structures. The robot could continue to function after being stepped on by an adult human (19.8 kg), a load about 9429 times its own body weight (Fig.15). Note that we used SCP actuators instead of SMA wires to improve the robustness.



Fig. 15. Weight-bearing capability. The robot's weight is 2.1 g. It can sustain an adult footstep of 19.8 kg force, a load about 9429 times its own body weight.

260 5 Conclusions

261 In this paper, we have introduced a new class of soft robots that leverage
262 contracting-cord particle jamming (CCPJ) to achieve self-assembly, shape mor-
263 phing, and stiffness modulation within a compact, integrated design. Our pri-
264 mary demonstration, TripodBot, exemplifies the capabilities of these robots,
265 showcasing their potential for applications in complex and remote environments.

266 The development of CCPJ-based soft robots represents a significant advance-
267 ment in the field of soft robotics. These robots offer numerous advantages, includ-
268 ing ease of fabrication, low cost, higher scalability, and robustness to punctures.
269 Additionally, they do not require bulky components like pumps and valves, mak-
270 ing them ideal for untethered operation in challenging environments.

271 Our work provides a practical framework for designing soft robots with en-
272 hanced adaptability and functionality. The integration of self-assembly, shape
273 morphing, and stiffness modulation within a single actuation system reduces
274 implementation complexity and weight, making these robots suitable for a wide
275 range of applications, from exploration in remote and hazardous areas to search
276 and rescue missions in confined spaces.

277 Several future directions aim to enhance TripodBot and more general CCPJ-
278 based robots: (1) Investigating new leg designs to eliminate reliance on ratchet
279 surfaces for locomotion, making the robot deployable in real-life scenarios and
280 unlocking omnidirectional movement due to its symmetric configuration. (2)
281 Developing new locomotion mechanisms to navigate uneven surfaces, increasing
282 versatility across various terrains. (3) Exploring alternative actuation options,
283 such as electromagnetic motors, to improve actuation frequency and energy effi-
284 ciency beyond the current thermal actuators (SMAs and SCP actuators), espe-
285 cially for larger-scale robots. (4) Creating a comprehensive analytical model to
286 optimize performance and make robot creation more accessible to the public. (5)
287 Current CCPJ-based robots can only have single, predefined shape morphing.
288 We will explore new strategies to achieve multiple shape self-deployment[25]. (6)
289 Integrating onboard sensing, control, and power systems to enable untethered
290 operation for field applications. By continuing to draw inspiration from biolog-
291 ical systems and leveraging advancements in material science and robotics, we
292 aim to develop even more capable and adaptable soft robotic systems.

293 In conclusion, embedding mechanical intelligence into robot bodies through
294 the incorporation of CCPJ introduces self-deployability, stiffness tuning, and
295 shape morphing, marking a promising step forward in the development of adap-
296 tive, self-deployable robotic systems. TripodBot serves as a compelling example
297 of the potential of these technologies, demonstrating their ability to navigate and
298 perform tasks in environments challenging for traditional robots. The continued
299 exploration and development of CCPJ mechanisms will undoubtedly open new
300 avenues for innovation and application in the field of soft robotics, contributing
301 significantly to the advancement of autonomous robotic solutions in diverse and
302 demanding settings.

303 References

- 304 1. Tianyu Chen, Xudong Yang, Bojian Zhang, Junwei Li, Jie Pan, and Yifan Wang.
305 Scale-inspired programmable robotic structures with concurrent shape morphing
306 and stiffness variation. *Science Robotics*, 9(92):eadl0307, 2024.
- 307 2. Samuel Felton, Michael Tolley, Erik Demaine, Daniela Rus, and Robert Wood. A
308 method for building self-folding machines. *Science*, 345(6197):644–646, 2014.
- 309 3. Wenzhong Yan, Talmage Jones, Christopher L Jawetz, Ryan H Lee,
310 Jonathan Brigham Hopkins, and Ankur Mehta. Self-deployable contracting-cord
311 metamaterials with tunable mechanical properties. *Materials Horizons*, 2024.
- 312 4. Emily Lathrop, Michael T Tolley, and Nick Gravish. Directionally compliant legs
313 enabling crevasse traversal in small ground-based robots. *Advanced Intelligent
314 Systems*, 5(4):2200258, 2023.
- 315 5. Kaushik Jayaram and Robert J Full. Cockroaches traverse crevices, crawl rapidly
316 in confined spaces, and inspire a soft, legged robot. *Proceedings of the National
317 Academy of Sciences*, 113(8):E950–E957, 2016.
- 318 6. Jiefeng Sun, Elisha Lerner, Brandon Tighe, Clint Middlemist, and Jianguo Zhao.
319 Embedded shape morphing for morphologically adaptive robots. *Nature Communi-
320 cations*, 14(1):6023, 2023.
- 321 7. Agostino Stilli, Helge A Wurdemann, and Kaspar Althoefer. Shrinkable, stiffness-
322 controllable soft manipulator based on a bio-inspired antagonistic actuation prin-
323 ciple. In *2014 IEEE/RSJ International Conference on Intelligent Robots and Sys-
324 tems*, pages 2476–2481. IEEE, 2014.
- 325 8. SP Murali Babu, Ali Sadeghi, Alessio Mondini, and Barbara Mazzolai. Antagonistic
326 pneumatic actuators with variable stiffness for soft robotic applications. In *2019
327 2nd IEEE International Conference on Soft Robotics (RoboSoft)*, pages 283–288.
328 IEEE, 2019.
- 329 9. Cecilia Laschi, Barbara Mazzolai, and Matteo Cianchetti. Soft robotics: Tech-
330 nologies and systems pushing the boundaries of robot abilities. *Science robotics*,
331 1(1):eaah3690, 2016.
- 332 10. Dohgyu Hwang, Edward J Barron III, ABM Tahidul Haque, and Michael D
333 Bartlett. Shape morphing mechanical metamaterials through reversible plastic-
334 ity. *Science robotics*, 7(63):eabg2171, 2022.
- 335 11. Carmel Majidi and Robert J Wood. Tunable elastic stiffness with microconfined
336 magnetorheological domains at low magnetic field. *Applied Physics Letters*, 97(16),
337 2010.
- 338 12. Kaspar Althoefer. Antagonistic actuation and stiffness control in soft inflatable
339 robots. *Nature Reviews Materials*, 3(6):76–77, 2018.
- 340 13. Bilige Yang, Robert Baines, Dylan Shah, Sreekalyan Patiballa, Eugene Thomas,
341 Madhusudhan Venkadesan, and Rebecca Kramer-Bottiglio. Reprogrammable
342 soft actuation and shape-shifting via tensile jamming. *Science Advances*,
343 7(40):eabh2073, 2021.
- 344 14. Vincent Wall, Raphael Deimel, and Oliver Brock. Selective stiffening of soft actu-
345 ators based on jamming. In *2015 IEEE International Conference on Robotics and
346 Automation (ICRA)*, pages 252–257. IEEE, 2015.
- 347 15. Yashraj S Narang, Joost J Vlassak, and Robert D Howe. Mechanically ver-
348 satile soft machines through laminar jamming. *Advanced Functional Materials*,
349 28(17):1707136, 2018.
- 350 16. Daniel Hasegawa, Buse Aktaş, and Robert D Howe. Tension jamming for deploy-
351 able structures. In *2023 IEEE/RSJ International Conference on Intelligent Robots
352 and Systems (IROS)*, pages 446–451. IEEE, 2023.

- 353 17. John R Amend, Eric Brown, Nicholas Rodenberg, Heinrich M Jaeger, and Hod
354 Lipson. A positive pressure universal gripper based on the jamming of granular
355 material. *T-RO*, 28(2):341–350, 2012.
- 356 18. Wenzhong Yan and Ankur Mehta. Towards one-dollar robots: An integrated de-
357 sign and fabrication strategy for electromechanical systems. *Robotica*, 41(1):31–47,
358 2023.
- 359 19. Xiaonan Huang, Kitty Kumar, Mohammad K Jawed, Amir M Nasab, Zisheng Ye,
360 Wanliang Shan, and Carmel Majidi. Chasing biomimetic locomotion speeds: Cre-
361 ating untethered soft robots with shape memory alloy actuators. *Science Robotics*,
362 3(25):eaau7557, 2018.
- 363 20. Jie Hong, Wenzhong Yan, Yanhong Ma, Dayi Zhang, and Xin Yang. Experimental
364 investigation on the vibration tuning of a shell with a shape memory alloy ring.
365 *Smart Mater. Struct.*, 24(10):105007, 2015.
- 366 21. Luyang Zhao, Yijia Wu, Wenzhong Yan, Weishu Zhan, Xiaonan Huang, Joran
367 Booth, Ankur Mehta, Kostas Bekris, Rebecca Kramer-Bottiglio, and Devin Balk-
368 com. Starblocks: Soft actuated self-connecting blocks for building deformable lat-
369 tice structures. *IEEE Robotics and Automation Letters*, 8(8):4521–4528, 2023.
- 370 22. Wenzhong Yan and Ankur Mehta. A crawling robot driven by a folded self-
371 sustained oscillator. In *2022 IEEE 5th International Conference on Soft Robotics*
(*RoboSoft*), pages 455–460. IEEE, 2022.
- 373 23. Yashraj S Narang, Alperen Degirmenci, Joost J Vlassak, and Robert D Howe.
374 Transforming the dynamic response of robotic structures and systems through
375 laminar jamming. *IEEE Robotics and Automation Letters*, 3(2):688–695, 2017.
- 376 24. Yichuan Wu, Justin K Yim, Jiaming Liang, Zhichun Shao, Mingjing Qi, Junwen
377 Zhong, Zihao Luo, Xiaojun Yan, Min Zhang, Xiaohao Wang, et al. Insect-scale
378 fast moving and ultrarobust soft robot. *Science robotics*, 4(32):eaax1594, 2019.
- 379 25. Rebecca Lin, Wenzhong Yan, Ankur Mehta, and Erik D Demaine. Routing recon-
380 figurations. In *ACM Symposium on Computational Fabrication*, SCF Adjunct ’24,
381 New York, NY, USA, 2024. Association for Computing Machinery.